ACS APPLIED MATERIALS & INTERFACES

Research Article

www.acsami.org

Graphene-Supported Ag-Based Core–Shell Nanoparticles for Hydrogen Generation in Hydrolysis of Ammonia Borane and Methylamine Borane

Lan Yang, Wei Luo,* and Gongzhen Cheng*

College of Chemistry, Molecular Sciences, Wuhan University, Wuhan, Hubei 430072, PR China

ABSTRACT: Well-dispersed magnetically recyclable core–shell Ag@M (M = Co, Ni, Fe) nanoparticles (NPs) supported on graphene have been synthesized via a facile in situ one-step procedure, using methylamine borane (MeAB) as a reducing agent under ambient condition. Their catalytic activity toward hydrolysis of ammonia borane (AB) were studied. Although the Ag@Fe/graphene NPs are almost inactive, the as-prepared Ag@Co/graphene NPs are the most reactive catalysts, followed by Ag@Ni/graphene NPs. Compared with AB and $NaBH_4$, the as-synthesized Ag@Co/graphene catalysts which reduced by MeAB exert the highest catalytic activity. Additionally, the Ag@Co NPs supported on graphene exhibit higher catalytic activity than the catalysts with other conventional supports, such as the SiO_2, carbon black, and γ-Al_2O_3. The as-synthesized Ag@Co/graphene NPs exert satisfied catalytic activity, with the turnover frequency (TOF) value of 102.4 (mol H_2 min^{-1} (mol Ag)$^{-1}$), and the activation energy E_a value of 20.03 kJ/mol. Furthermore, the as-synthesized Ag@Co/graphene NPs show good recyclability and magnetically reusability for the hydrolytic dehydrogenation of AB and MeAB, which make the practical reusing application of the catalysts more convenient. Moreover, this simple synthetic method indicates that MeAB could be used as not only a potential hydrogen storage material but also an efficient reducing agent. It can be easily extended to facile preparation of other graphene supported metal NPs.

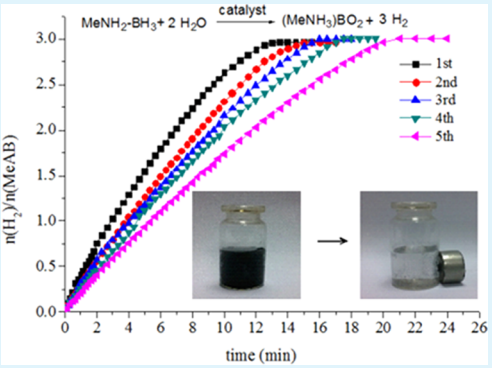

KEYWORDS: *core–shell NPs, ammonia borane, methylamine borane, graphene, hydrogen storage*

1. INTRODUCTION

Bimetallic core–shell nanoparticles (NPs) have attracted considerable interests for their unique optical, electronic, magnetic, and catalytic properties.[1−4] Because of the interplay of electronic and lattice effects of the neighboring metals,[5] the catalytic activity of the core–shell NPs are superior to the alloy and monometallic counterparts. The catalytic performance of the metal NPs is highly dependent on the dispersion of the active metals. Hence, to prevent the NPs from aggregation, appropriate supports have been designed for restraining the agglomeration of the metal NPs. Graphene, a single-layer of sp^2 carbon lattices, holding many advantages such as outstanding charge carrier mobility,[6] thermal and chemical stability,[7] high specific surface area,[8] superior electrical conductivity,[9] etc., could be an ideal substrate for growing and anchoring metal NPs. It has been reported that the enhanced catalytic activity of the graphene supported metal NPs is mainly caused by the charge transfer across the graphene–metal interface, because of the graphene–metal spacing and Fermi lever difference.[10] The most commonly used method to make the graphene-supported metal NPs was the two-step ex situ way, which involves reducing graphite oxide (GO) and metal precursors first, and then depositing the metal NPs onto the graphene. In this way, the complicated reaction steps, long reaction time, and stringent reaction conditions (high temperature, high vacuum, microwave, ultrasound, UV irradiation, etc.) are usually unavoidable.[11−15] Therefore, developing a mild and rapid strategy for the facile one-step synthesis of graphene supported core–shell NPs with high catalytic activity at room temperature still remains considerable challenge.

Hydrogen, producing only water as a byproduct, has emerged as one of the potential carbon-neutral energy carrier alternatives. Currently, a great deal of work has been devoted to the development of effective hydrogen storage materials for hydrogen fuel cells and hydrogen energy systems, including metal hydrides,[16] sorbent materials,[17] and chemical hydride systems.[18] Having been used as hydrogen storage materials, boron–nitrogen-containing compounds have attracted many concerns because of their high gravimetric hydrogen densities and favorable kinetics of hydrogen release.[19] Ammonia borane (NH_3–BH_3, AB), with 19.6 wt % hydrogen content, is highly stable, environmentally benign, and accordingly an attractive candidate for chemical hydride systems.[20] The release of hydrogen from AB could be obtained via thermal decomposition,[21] catalytic dehydrogenation in nonaqueous solvent,[22] and hydrolysis.[23] With appropriate catalyst, hydrolysis of AB can release 3 mol of H_2 per mol AB at room temperature, which appears to be the most convenient one for portable

Received: June 19, 2013
Accepted: July 26, 2013
Published: July 26, 2013

hydrogen storage applications.[24−29] So far, not only noble and non-noble metal NPs but also their composites were tested for hydrolytic dehydrogenation of AB. However, as a derivative of AB, methylamine borane (CH_3NH_2−BH_3, MeAB) has not been widely studied. It could release hydrogen from 120 to 210 °C within 100 min,[30] and in THF at 20 °C by Ir and Ru catalysts.[31] As far as we know, there are no reports on hydrolysis of MeAB, which could also release 3 mol of H_2 per mol MeAB at room temperature according to eq 1.

$$MeNH_2 - BH_3 + 2H_2O \xrightarrow{\text{catalyst}} (MeNH_3)BO_2 + 3H_2 \quad (1)$$

Moreover, as the classical Lewis acid−base adducts, amine−boranes offer much better control in reducing rate and selective reduction of metal ions over the traditional reducing agents like borohydrides.[32] The reducing strength decreases when increasing the alkyl substitution on nitrogen: H_3N-BH_3> $MeNH_2$−BH_3> Me_2NH-BH_3> Me_3N-BH_3. However, they have not been widespread used as reducing agents in the synthesis of metal NPs.[33] Therefore, exploring a new strategy to develop efficient, economical, and stable catalysts toward hydrogen generation is highly desirable.

In this work, we report a facile in situ coreduction method for preparing graphene supported Ag@M (M = Co, Ni, Fe) NPs with methylamine borane (MeAB) as the reducing agent under ambient conditions. Their catalytic activity toward hydrolytic dehydrogenation of AB and MeAB under ambient conditions have been studied.

2. EXPERIMENTAL SECTION

2.1. Materials. Ammonia borane (NH_3−BH_3, AB, Aldrich, 90%), sodium borohydride (Sinopharm Chemical Reagent Co., Ltd., ≥96%), cobalt nitrate hexahydrate ($Co(NO_3)_2{\cdot}6H_2O$, Sinopharm Chemical Reagent Co., Ltd., ≥99%), nickel(II) nitrate hexahydrate ($Ni(NO_3)_2{\cdot}6H_2O$, Sinopharm Chemical Reagent Co., Ltd., AR), ferric nitrate nonahydrate ($Fe(NO_3)_3{\cdot}9H_2O$, Sinopharm Chemical Reagent Co., Ltd., ≥99%), silver nitrate ($AgNO_3$, AR), methylamine hydrochloride ($CH_3NH_2{\cdot}HCl$, Sinopharm Chemical Reagent Co., Ltd., ≥96%), potassium permanganate ($KMnO_4$, Shanghai Chemic Co., Ltd., ≥99.5%), hydrogen peroxide (H_2O_2, Sinopharm Chemical Reagent Co., Ltd., ≥30%), sodium nitrate ($NaNO_3$, Sinopharm Chemical Reagent Co., Ltd., ≥99%), sulfuric acid (H_2SO_4, Sinopharm Chemical Reagent Co., Ltd., 95−98%), tetrahydrofuran (C_4H_8O, Sinopharm Chemical Reagent Co., Ltd., ≥99%), dimethyl ether anhydrous ($C_4H_{10}O$, Sinopharm Chemical Reagent Co., Ltd., ≥99.7%), graphite power (Sinopharm Chemical Reagent Co., Ltd., ≥99.85%), aluminum oxide (Al_2O_3, Sinopharm Chemical Reagent Co., Ltd., FCP), neutral silica power (SiO2, Branch of Qingdao Haiyang Chemical Co., Ltd., LR), and carbon black (EC-300J, Triquo Chemical Co., Ltd.) were used as obtained. We use ordinary distilled water as the reaction solvent.

2.2. Graphite Oxide (GO) Preparation. GO was made by a modified Hummers method.[34,35] In a typical synthesis of graphite oxide, 1.0 g of natural graphite flakes was dispersed in 50.0 mL of H_2SO_4 in a 500 mL flask. Then, 1.0 g of $NaNO_3$ was added into the mixture under continuous stirring . The flask was placed into the ice-bath to decrease the reaction temperature in the range of 0−3 °C because an exothermic reaction occurs upon addition of $KMnO_4$ in the following step. Once everything has been settled down, 6.0 g of $KMnO_4$ was added partially by controlling the temperature of the reaction via a thermometer placed into the reaction mixture. Then, the resulting mixture was stirred for 30 min in the ice-bath. After the removal of the ice-bath, the solution was heated to 35 °C and stirred for 3 h. A thick paste was formed after 3 h stirring at 35 °C. The solution was then placed in ice-bath again and 50.0 mL of water was added dropwise.

A dark-brown slurry was formed after the solution was stirred for 30 min at room temperature. Finally, 100 mL of water and 8.0 mL of 30% H_2O_2 were added dropwise into the dark-brown slurry and the addition of 2.0 mL of excess H_2O_2 was followed until observation of a permanent yellow color, which indicating the complete oxidation of graphite. The resultant solution was centrifuged to obtain the product. Centrifuged product was washed by deionized water, diluted hydrochloric acid, and absolute ethyl alcohol many times and then dried under vacuum at 25 °C.

2.3. Preparation of Methyl Ammonia Borane (CH_3NH_2−BH_3, MeAB). MeAB was synthesized by the method reported in the literature.[36] Sodium borohydride (3.783 g, 0.1 mol) and methylamine hydrochloride (6.752 g, 0.1 mol) were added to a 500 mL two-neck round-bottom flask with a neck connected to a condenser. THF (200 mL) was transferred into the flask with vigorously stirring. The reaction was carried out at room temperature under nitrogen atmosphere. After 12 h, the resultant solution was filtered by suction filtration and the filtrate was concentrated under vacuum at room temperature. The product was purified by diethyl ether.

2.4. In Situ Synthesis of Ag@Co/Graphene, Ag@Ni/Graphene, Ag@Fe/Graphene NPs and Their Catalytic Studies of Hydrolytic Dehydrogenation of AB. In a typical experiment, 10 mg of GO was dissolved in 5 mL of water, and kept in a 25 mL two-necked round-bottom flask. Ultrasonication was required to get a uniform dispersion solution. Two milliliters of cobalt nitrate (or nickel nitrate, or ferric nitrate nonahydrate) solution (0.0225 mol/L) and 0.1 mL of silver nitrate solution (0.05 mol/L) were added into the round-bottom flask. One neck was connected to a gas buret, and the other one was connected to a pressure-equalization which used to introduce MeAB. 2.0 mL of aqueous solution containing 90.0 mg MeAB (2 mmol) was kept in the pressure-equalization. The reactions were started when the MeAB solution was added to the flask with vigorously stirring, the evolution of the gas was monitored by the gas buret. When the hydrogen generation reaction was completed, 2.0 mL of aqueous solution containing 1 mmol AB was added to the flask, the evolution of the gas was monitored. A water bath was used to control the temperature of the reaction solution.

In order to find an optimized reaction condition for catalytic dehydrogenation of AB, the molar ratio of Ag/Co or Ag/Ni were varied from 0 to 1, whereas the molar ratio for catalysts to AB was kept as a constant of 0.05.

For comparison, Ag@Co/graphene NPs reduced by AB and AgCo/graphene NPs reduced by $NaBH_4$ were synthesized respectively by the similar method.

2.5. Different Supported Materials. Sets of experiments with/without 10 mg different supported materials (such as SiO_2, γ-Al_2O_3 and carbon black) were performed at room temperature (25 ± 0.2 °C). All the experiments were performed in the same way as described in the section 2.4.

2.6. Kinetic Studies of Hydrolytic Dehydrogenation of AB Catalyzed by $Ag_{0.1}@Co_{0.9}$/Graphene and $Ag_{0.1}@Ni_{0.9}$/Graphene NPs. Sets of experiments with different amounts of Ag@Co/graphene (or Ag@Ni/graphene) (0.04, 0.05, 0.06, 0.07 mmol) NPs were performed at room temperature (25 ± 0.2 °C), while AB was kept the same (1 mmol) to determine the rate law of the catalytic hydrolysis of AB. Temperature was varied at 25 ± 0.2 °C, 30 ± 0.2 °C, 35 ± 0.2 °C, and 40 ± 0.2 °C while keeping the molar ratio of catalyst/AB as 0.05 to obtain the activation energy (E_a).

2.7. Reusability and Recyclability Test of $Ag_{0.1}@Co_{0.9}$/Graphene NPs for the Hydrolysis of AB and MeAB. The reusability test was processed by the method reported in the literature.[37] After the first hydrogen generation was completed, the in situ as-synthesized catalysts were magnetically attracted to the bottom of the reaction flask by a magnet, and the upper solution was removed. For recyclability test, catalytic reactions were repeated 5 times by adding another equivalent of AB or MeAB (1 mmol) into the mixture after the previous cycle. The molar ratio of catalyst/AB was kept for 0.05.

2.8. Characterization. TEM images were obtained using a FEI Tecnai G20 TEM instrument operating at 200 kV. Powder X-ray

diffraction (XRD) patterns were measured by a Bruker D8-Advance X-ray diffractometer using Cu Ka radiation source (λ = 0.154178 nm) with a velocity of 6° min^{-1}. FTIR spectra were collected at room temperature by using a Thermo FTIR-iS10 instrument using KBr discs in the 400−4000 cm^{-1} region. Raman spectra were carried out using a confocal Raman microscope (Renishaw, RM-1000) at 514.5 nm excitation. X-ray photoelectron spectroscopy (XPS) measurement was performed with a Kratos XSAM 800 spectrophotometer. ^{11}B NMR spectra were recorded on a Varian-VX 300 spectrometer at ambient temperature, and externally referenced to $BF_3{\cdot}Et_2O$ (δ = 0).

3. RESULTS AND DISCUSSION

3.1. Synthesis and Characterization. In a typical synthesis of graphene-supported Ag@M (M = Co, Ni, Fe) core−shell NPs, to a round-bottom flask containing a mixture aqueous solution of $AgNO_3$, $Co(NO_3)_2$ or $Ni(NO_3)_2$ or $Fe(NO_3)_2$, and graphene oxide (GO), the methylamine borane solution was introduced. Considering the lower reduction potentials ($E^0(Co^{2+}/Co)$ = −0.28 eV vs. SHE; $E^0(Ni^{2+}/Ni)$ = −0.25 eV vs. SHE; $E^0(Fe^{2+}/Fe)$ = −0.44 eV vs. SHE), M^{2+} cannot be directly reduced by MeAB. The Ag^+ with high reduction potential ($E^0(Ag^+/Ag)$ = +0.80 eV vs. SHE) was first reduced by MeAB to form the Ag NPs, and serving as the in situ seeds to induce the successive growth of the M NPs as the shell, which may be generated by the Ag−H species with strong reducing ability,[38] to form the Ag@M core−shell NPs.

The microstructures of Ag@Co/graphene, Ag@Ni/graphene, and Ag@Co NPs were characterized by transmission electron microscopy (TEM). As shown in images a and d in Figure 1, the as-synthesized NPs were well-dispersed on

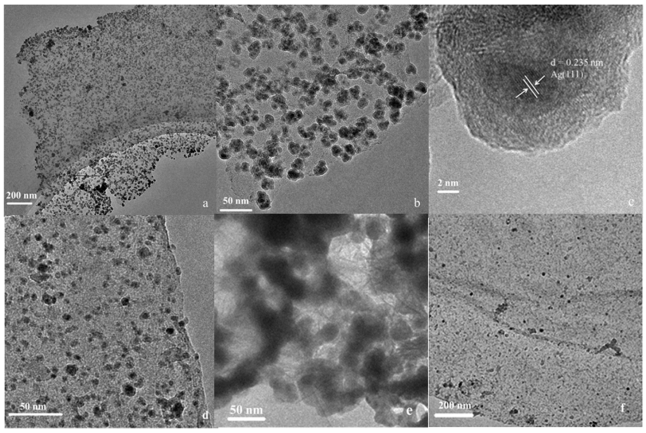

Figure 1. TEM images of (a−c) Ag@Co/graphene NPs; (d) Ag@Ni/graphene NPs; (e) Ag@Co NPs; (f) Ag@Co/graphene NPs after fifth run.

graphene, which helps to prevent the agglomeration. The Ag@Co NPs without graphene were observed severe agglomeration (Figure 1e), which may hinder the active sites and decrease the reaction activity (vide infra). A distinct contrast of core and shell can be observed clearly by the high-resolution TEM (HRTEM), as shown in Figure 1c; the dark core is Ag, and the gray shell is Co, indicating that Ag is initially reduced by MeAB, and subsequently acts as the seed helping for reducing of Co^{2+} to form the shell. The *d*-spacing of the crystallized core part is ~0.235 nm, which is consistent with the Ag(111) plane spacing. Figure 2 shows the power XRD pattern of the as-prepared Ag@Co/graphene and Ag@Ni/graphene NPs, in which the diffraction peaks attributed to Ag(111) are observed.

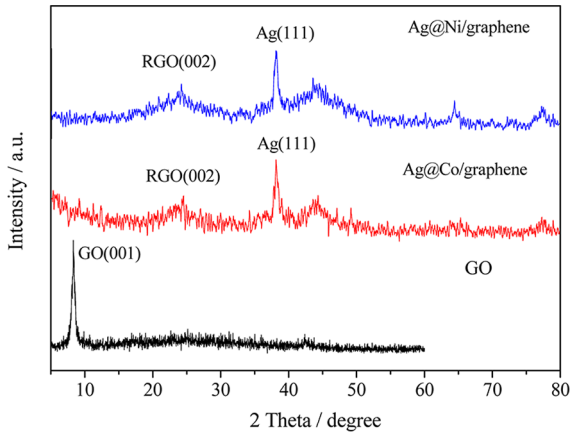

Figure 2. XRD patterns of GO, Ag@Co/graphene, and Ag@Ni/graphene.

However, no diffraction peaks of Co and Ni exit, which may be caused by the amorphous phase of Co and Ni. Furthermore, the most intense peak at around 8.4° corresponds to the GO disappeared, while a new peak at around 23.9° is observed in the as-prepared graphene supported NPs, indicating that the GO is successfully reduced to graphene. In the Raman spectroscopy (Figure 3), the GO and graphene supported

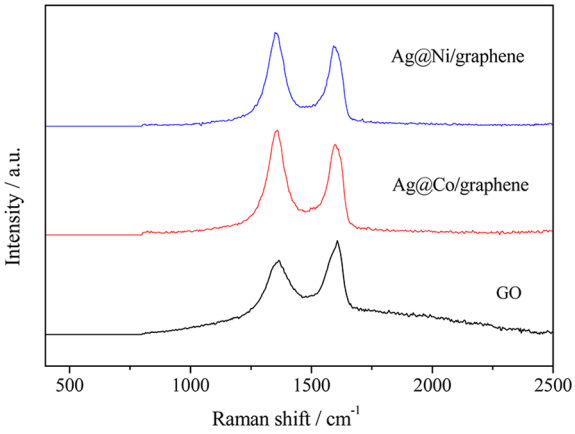

Figure 3. Raman spectra of GO, Ag@Co/graphene, and Ag@Ni/graphene.

NPs exhibit two peaks centered at 1358 and 1596 cm^{-1}, corresponding to the D and G bands of the carbon products, respectively. The intensity ratio of the D to G band (I_D/I_G) is generally accepted to reflect the degree of graphitization of carbonaceous materials and defect density. After loading of the Ag@Co and Ag@Ni NPs, the I_D/I_G of GO are both increased from 1.01 to 1.32. The relative changes in the D to G peak intensity ratio confirm the reduction of GO during the in situ fabrication. Figure 4 shows the FTIR spectra of GO and graphene-supported Ag@Co and Ag@Ni core−shell NPs. The disappearance of the C═O peak at 1634 cm^{-1}, C−OH peak at 1227 cm^{-1}, and C−O peak at 1057 cm^{-1} of GO after the formation of graphene supported core−shell NPs can clearly be seen, further indicating the GO was reduced to graphene during the process.

3.2. Catalytic Activity for Hydrolysis of AB by Ag@Co/Graphene NPs. The as-synthesized Ag@Co/graphene NPs with different composition have been tested for hydrolysis of

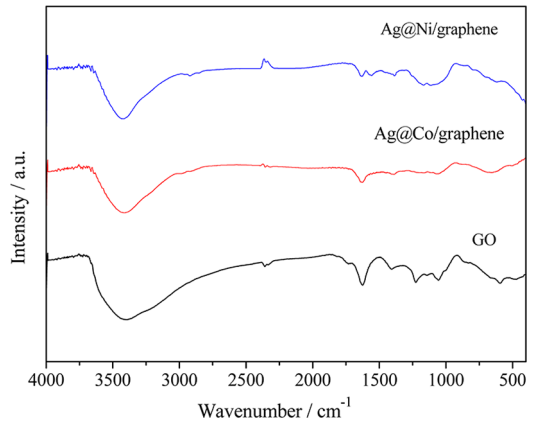

Figure 4. FTIR spectra of GO, Ag@Co/graphene, and Ag@Ni/graphene.

AB. Without Ag addition, the precursor Co cannot be reduced by using MeAB as reducing agent. As shown in Figure 5, by

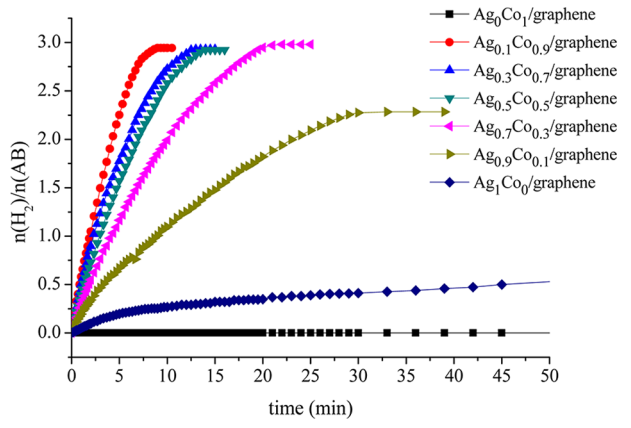

Figure 5. Hydrogen generation profile from the hydrolysis of AB catalyzed by $Ag_x@Co_{1-x}$/graphene (x = 0, 0.1, 0.3, 0.5, 0.7, 0.9, and 1) at 25 ± 0.2 °C, [cat]/[AB] = 0.05.

changing the Ag molar ratio, the $Ag_x@Co_{1-x}$ NPs demonstrate different catalytic activity. Unexpectedly, as the molar ratio of Ag (x value) increases from 0.1 to 1.0, the catalytic activity of the as-synthesized NPs decrease gradually, and AB cannot be catalytic decomposed completely when the Ag increase to 0.9. Although only Ag NPs were supported on graphene, less than 1.5 equiv. of H_2 was released over 5 h, indicating the positive effect of metal interaction in the bimetallic Ag@Co core−shell NPs on hydrogen generation from hydrolysis of AB. This is similar to Zhang and co-worker's report on Pd@Co/graphene system.[39] As a result, the best ratio in $Ag_x@Co_{1-x}$ system is $Ag_{0.1}@Co_{0.9}$, which may be attributed to more active sites deriving from the higher amorphous Co contents.[40] The activity in terms of turnover frequency (TOF) is 102.4 (mol H_2 min^{-1} (mol Ag)$^{-1}$) for the as-synthesized $Ag_{0.1}@Co_{0.9}$/graphene NPs, this value is the highest value ever reported among the Ag-based catalysts, and higher than that of most reported noble metal-based NPs, if the TOF is normalized in terms of mol noble metal (Table 1). Figure 6 shows time courses of hydrogen evolution from aqueous AB solutions catalyzed by $Ag_{0.1}@Co_{0.9}$/graphene catalysts with different amount of GO at 25.0 ± 0.3 °C. With increasing GO, the catalytic performance increases, while GO continues to

Table 1. Catalytic Activity of Different Noble Metal-Based Catalysts Used for the Hydrolytic Dehydrogenation of AB

catalyst	TOF (mol H_2 mol^{-1} M min^{-1}) M = Ru, Pd, Ag	E_a (kJ mol^{-1})	ref
$Ni_{0.74}Ru_{0.26}$ alloy NPs	194.8	44	41
PSSA-co-MA stabilized Ru nanoclusters	187.6	54	42
Ni@Ru	114		43
Ag@Co/graphene	102.4	20.03	this study
Ag@Ni/graphene	77.0	49.56	this study
laurate-stabilized Ruthenium(0) nanoclusters	75	47 ± 2.2	44
$Ru@Al_2O_3$	39.6	48 ± 2	28
RuCo (1:1)/γ-Al_2O_3	32.9	47	45
Ru/γ-Al_2O_3	23.05	67	46
PSSA-co-MA stabilized Pd nanoclusters	19.9	44	42
RuCu (1:1)/γ-Al_2O_3	16.4	52	45
Ag@C@Co	8.93		47
RGO/Pd	6.25	51	48
Ag/C/Ni	5.32	38.91	49

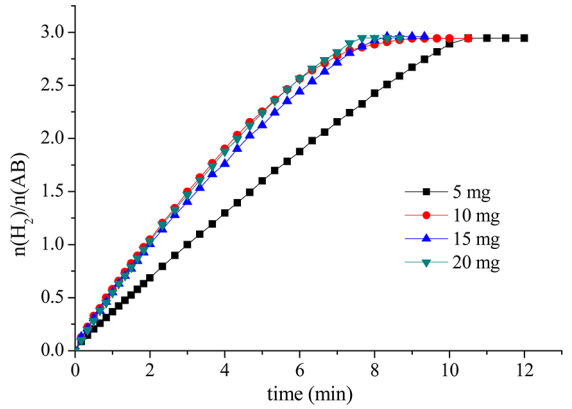

Figure 6. H_2/NH_3BH_3 molar ratio of hydrogen generated from the hydrolysis of AB catalyzed by $Ag_{0.1}@Co_{0.9}$/graphene NPs with different amount of GO (5, 10, 15, 20 mg), catalyst/AB = 0.05.

increase, there is no significant decrease in catalytic time, indicating the best amount of GO in our system is 10 mg.

For comparison, $Ag_{0.1}@Co_{0.9}$/graphene NPs generated by AB as reducing agent and $Ag_{0.1}Co_{0.9}$/graphene alloy NPs reduced by $NaBH_4$ are also prepared and applied to catalytic hydrolysis of AB. As shown in Figure 7, their catalytic activity are both inferior to that of $Ag_{0.1}@Co_{0.9}$/graphene NPs reduced by MeAB, which confirms that it is possible to achieve much better control over the nucleation and growth process over the graphene by changing the reducing agents, and further affect their catalytic activity. Additionally, to study the effects of the supported materials on the catalytic performances of the as-synthesized core−shell NPs, we prepared $Ag_{0.1}@Co_{0.9}$/C, $Ag_{0.1}@Co_{0.9}/SiO_2$, $Ag_{0.1}@Co_{0.9}/\gamma$-Al_2O_3, and graphene-free $Ag_{0.1}@Co_{0.9}$ NPs and studied their catalytic activity toward hydrolysis of AB. As shown in Figure 8, their catalytic activity are both inferior to that of $Ag_{0.1}@Co_{0.9}$/graphene NPs, highlighting the dominant factor of graphene in facilitating hydrolysis of AB in our system.

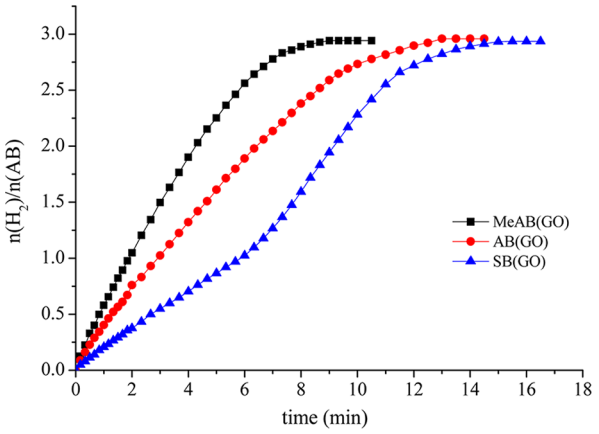

Figure 7. Time plots of catalytic dehydrogenation of AB by $Ag_{0.1}$@$Co_{0.9}$/graphene NPs reduced by MeAB and AB, and $Ag_{0.1}Co_{0.9}$/graphene reduced by $NaBH_4$ respectively, catalyst/AB = 0.05.

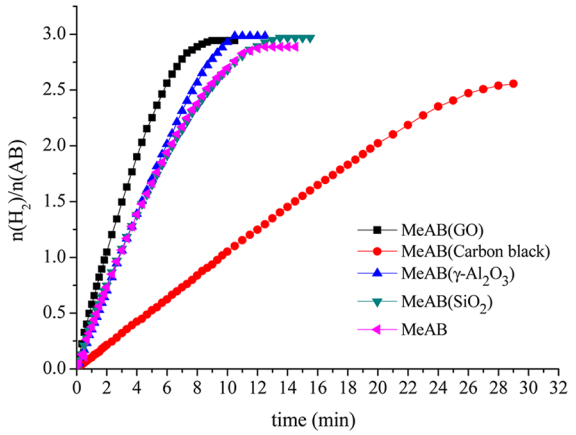

Figure 8. Time plots of catalytic dehydrogenation of AB by $Ag_{0.1}$@$Co_{0.9}$ NPs reduced by MeAB with/without supported materials, catalyst/AB = 0.05.

Figure 9 shows the plots of hydrogen generation from the hydrolysis of AB solution in the presence of different $Ag_{0.1}$@$Co_{0.9}$/graphene NPs concentrations at 25 ± 0.2 °C. The initial rate of hydrogen generation was determined from the initial nearly linear portion of each plot. The line slope of the plot of hydrogen evolution rate versus catalyst concentration in a log−log scale is 1.15, indicating that the hydrolysis of AB catalyzed by $Ag_{0.1}$@$Co_{0.9}$/graphene NPs is first order with respect to the catalyst concentration.

To get the activation energy (E_a) of the AB hydrolysis catalyzed by $Ag_{0.1}$@$Co_{0.9}$/graphene NPs, the hydrolytic reactions at different temperature range of 25−40 °C were carried out. The values of rate constant k at different temperatures were calculated from the slope of the linear part of each plot from Figure 10a. The Arrhenius plot of ln k vs $1/T$ for the catalyst is plotted in Figure 10b, from which the apparent activation energy was determined to be approximately 20.03 kJ/mol, being lower than most of the reported E_a values (Table 1), indicating the superior catalytic performance of the as-synthesized $Ag_{0.1}$@$Co_{0.9}$/graphene NPs.

3.3. Catalytic Activity for Hydrolysis of AB by Ag@Ni/Graphene NPs. The as-synthesized Ag@Ni/graphene NPs with different composition have been tested for hydrolysis of AB. Without Ag addition, the precursor Ni cannot be reduced by using MeAB as reducing agent. As shown in Figure 11, by changing the Ag molar ratio, the Ag_x@Ni_{1-x} NPs demonstrate different catalytic activity. Similar to Ag@Co/graphene NPs, as the molar ratio of Ag (x value) increases from 0 to 1.0, the catalytic activity of the Ag_x@Ni_{1-x} NPs decrease gradually, and AB cannot be catalytic decomposed completely when the Ag increase to 0.7. As a result, the best ratio in Ag_x@Ni_{1-x} system is $Ag_{0.1}$@$Ni_{0.9}$. The activity in terms of turnover frequency (TOF) is 77.0 (mol H_2 min^{-1} (mol Ag)$^{-1}$) for the as-synthesized $Ag_{0.1}$@$Ni_{0.9}$/graphene NPs, this value is smaller than that of $Ag_{0.1}$@$Co_{0.9}$/graphene NPs, but still higher than that of most reported noble metal-based NPs, if the TOF is normalized in terms of mol noble metal (Table 1). For comparison, $Ag_{0.1}$@$Fe_{0.9}$/graphene NPs were synthesized using the similar method. From Figure 11, the as-prepared $Ag_{0.1}$@$Fe_{0.9}$/graphene NPs show almost no reactivity toward hydrolysis of AB, and even worse than Ag/graphene NPs, indicating the negative effect of Fe in our system toward the dehydrogenation of AB at ambient conditions.

Figure 12 shows the plots of hydrogen generation from the hydrolysis of AB solution in the presence of different $Ag_{0.1}$@$Ni_{0.9}$/graphene NPs concentrations at 25 ± 0.2 °C. The initial rate of hydrogen generation was determined from the initial nearly linear portion of each plot. The line slope of the plot of

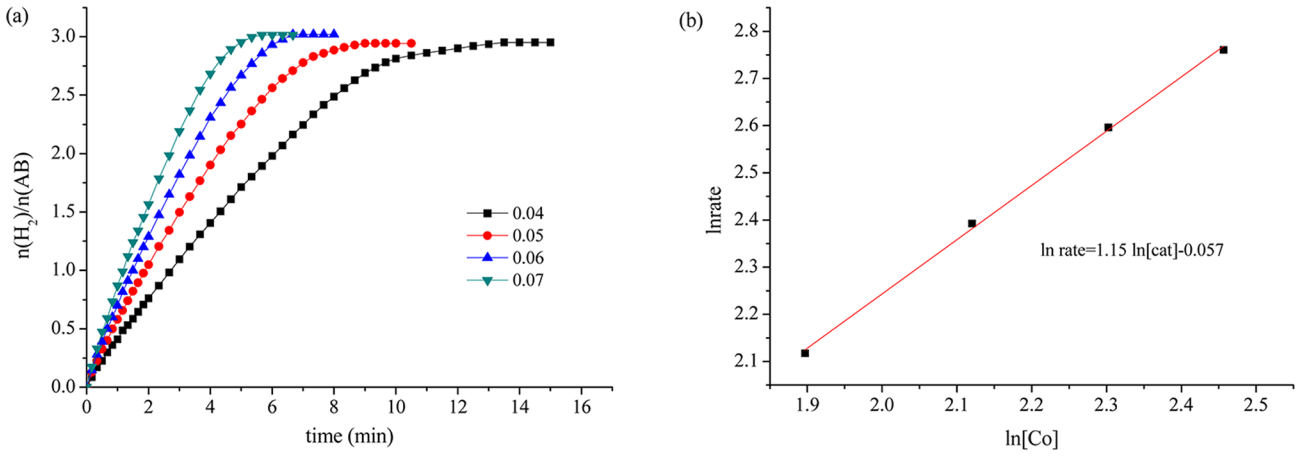

Figure 9. (a) Time plots of mol H_2 per mol AB vs time for $Ag_{0.1}$@$Co_{0.9}$/graphene catalyzed hydrolysis of AB at different catalyst concentration; (b) plot of hydrogen generation rate vs. the concentration of $Ag_{0.1}$@$Co_{0.9}$/graphene (both in logarithmic scale).

dx.doi.org/10.1021/am402373p | ACS Appl. Mater. Interfaces 2013, 5, 8231−8240

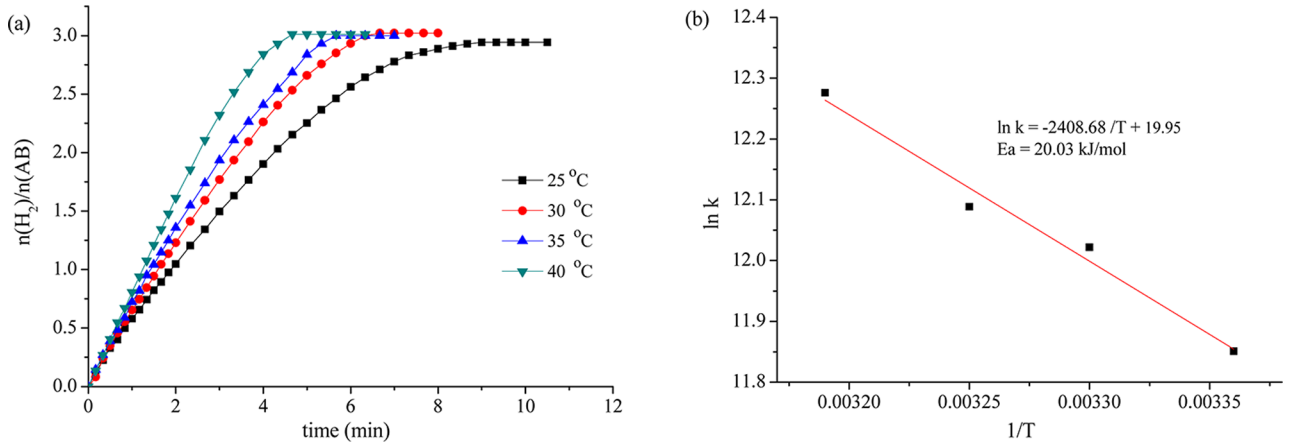

Figure 10. (a) Time plots of mol H_2 per mol AB vs time for $Ag_{0.1}@Co_{0.9}$/graphene catalyzed hydrolysis of AB at four different temperatures in the range of 25−40 °C, catalyst/AB = 0.05; (b) Arrhenius plot obtained from the data in panel a.

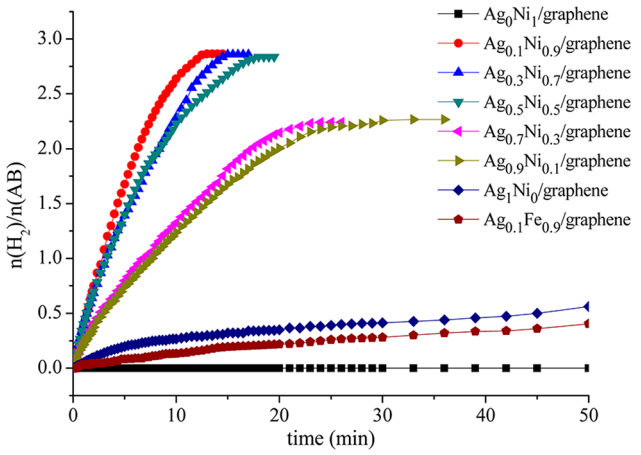

Figure 11. Hydrogen generation profile from the hydrolysis of AB catalyzed by $Ag_x@Ni_{1-x}$/graphene (x = 0, 0.1, 0.3, 0.5, 0.7, 0.9, and 1), and $Ag_{0.1}@Fe_{0.9}$/graphene NPs at 25 ± 0.2 °C, [cat]/[AB] = 0.05.

hydrogen evolution rate versus catalyst concentration in a log−log scale is 1.06, indicating that the hydrolysis of AB catalyzed by $Ag_{0.1}@Ni_{0.9}$/graphene NPs is first order with respect to the catalyst concentration.

To get the activation energy (E_a) of the AB hydrolysis catalyzed by $Ag_{0.1}@Ni_{0.9}$/graphene NPs, the hydrolytic reactions at different temperature range of 25−40 °C were carried out. The values of rate constant k at different temperatures were calculated from the slope of the linear part of each plot from Figure 13a. The Arrhenius plot of ln$k$ vs 1/T for the catalyst is plotted in Figure 13b, from which the apparent activation energy was determined to be approximately 49.56 kJ/mol, which is higher than the $Ag_{0.1}@Co_{0.9}$/graphene NPs.

3.4. Reusability and Recycle Ability. The reusability of the catalyst is crucial in the practical application. Figure 14 shows the reusability of the $Ag_{0.1}@Co_{0.9}$/graphene NPs up to fifth run for hydrolysis of AB, the catalysts retain 49.7% of their initial catalytic activity in the hydrolysis of AB in the fifth run. The recyclability of $Ag_{0.1}@Co_{0.9}$/graphene NPs up to fifth run for hydrolysis of AB and MeAB are shown in Figure 15 and 16 respectively. As shown in Figure 15, the as-prepared $Ag_{0.1}@Co_{0.9}$/graphene catalysts retain 52.5% of their initial catalytic activity in the hydrolysis of AB in the fifth run. In Figure 16, with our as-synthesized bimetallic core−shell $Ag_{0.1}@Co_{0.9}$/graphene NPs, MeAB can release 3 equiv. of H_2 in less than 12 min at room temperature, with turnover frequency (TOF) value of 70.6 (mol H_2 min^{-1} (mol Ag)$^{-1}$), and retain 56.4% of their initial catalytic activity after the fifth cycle. Furthermore, the as-synthesized $Ag_{0.1}@Co_{0.9}$/graphene NPs are magnetic and thus can be separated from the reaction solution by an external

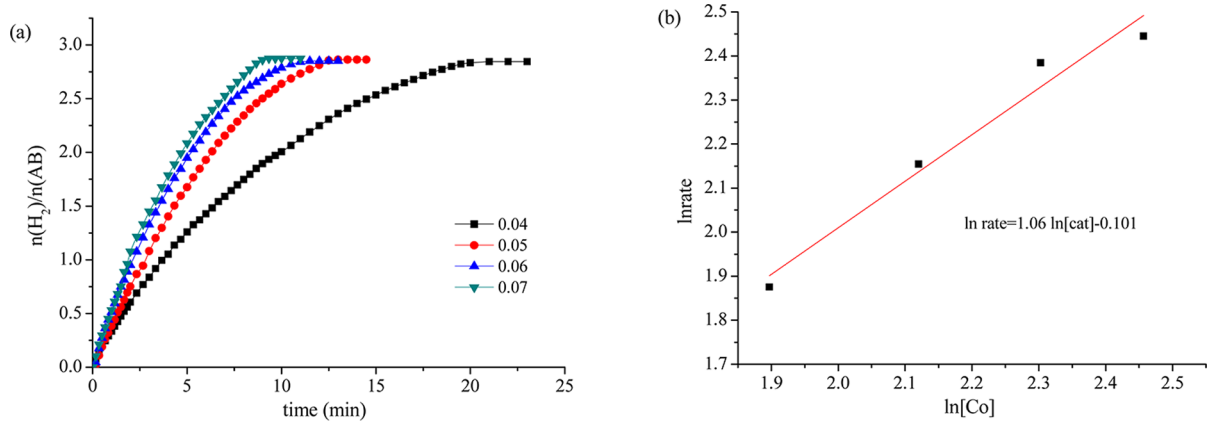

Figure 12. (a) Time plots of mol H_2 per mol AB vs. time for $Ag_{0.1}@Ni_{0.9}$/graphene catalyzed hydrolysis of AB at different catalyst concentration; (b) plot of hydrogen generation rate vs the concentration of $Ag_{0.1}@Ni_{0.9}$/graphene (both in logarithmic scale).

dx.doi.org/10.1021/am402373p | ACS Appl. Mater. Interfaces 2013, 5, 8231−8240

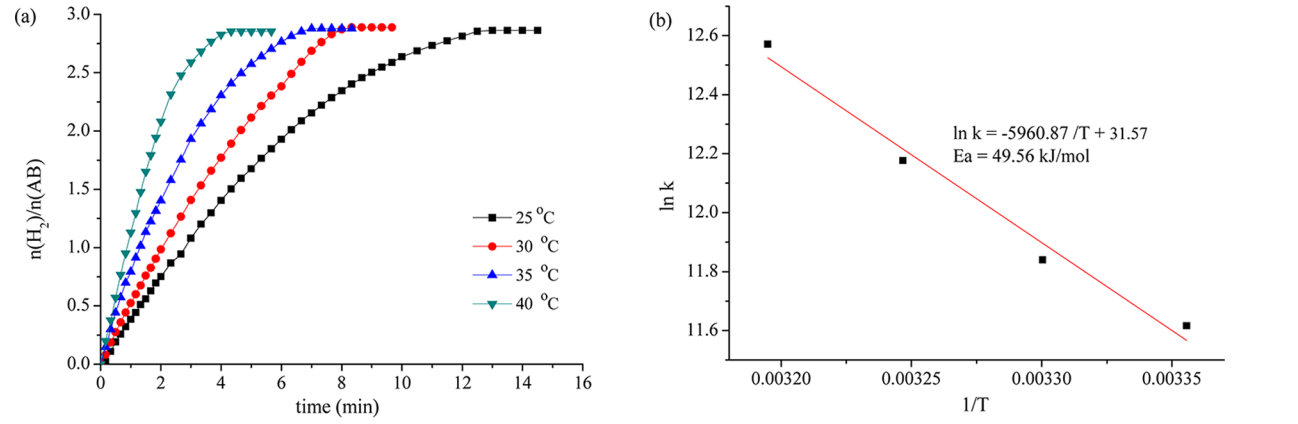

Figure 13. (a) Time plots of mol H_2 per mol AB vs time for $Ag_{0.1}@Ni_{0.9}$/graphene catalyzed hydrolysis of AB at four different temperatures in the range of 25−40 °C, catalyst/AB = 0.05; (b) Arrhenius plot obtained from the data in panel a.

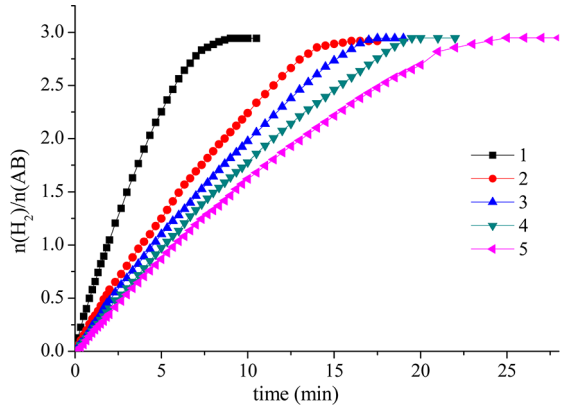

Figure 14. Hydrogen generation from the hydrolysis of AB catalyzed by $Ag_{0.1}@Co_{0.9}$/graphene NPs in the catalysts reusability test, catalyst/AB = 0.05.

magnet (Figure 16a inset), which makes the practical recycling application of the NPs more convenient. Figure 1f shows a representative TEM image of $Ag_{0.1}@Co_{0.9}$/graphene NPs after the fifth run recyclability test. As clearly seen from the TEM image, there is no agglomeration of the as-synthesized NPs on graphene. This indicates that the graphene can stabilize the as-synthesized $Ag_{0.1}@Co_{0.9}$/graphene NPs at least for five cycles.

Figure 17 shows the XPS of the GO, and $Ag_{0.1}@Co_{0.9}$/graphene catalysts before and after five cycles. Compared with the peaks of GO (Figure 17a), the intensities of the oxygen containing functional groups (such as −C−O, −C═O, −COO) in $Ag_{0.1}@Co_{0.9}$/graphene (Figure 17b) decrease significantly,[26] which also reveal the reduction of GO to graphene. Panels c and d in Figure 17 show the XPS peak of Ag 3d of the catalysts before and after five cycles. The two peaks are 368.2 and 374.2 eV, these values are in good agreement with the values for zerovalent Ag, standing for Ag $3d_{5/2}$ and Ag $3d_{3/2}$. There are almost no differences between the two peaks before and after five cycles, illustrating that Ag is not oxidized as the core. Figure 17e shows the peaks of Co 2p after five cycles. There are three peaks whose peak tops are 778.5, 780.6, and 786.3 eV, which stand for Co^0 and oxidized Co, respectively. These results indicate that the core Ag metal is stable, whereas the outside shell of Co is partly oxidized during the catalytic process. Therefore, the decrease in the catalytic activity may be due to the oxidization of the shell parts of the catalysts. Meanwhile, the increased viscosity of the solution and deactivation effect of the increasing metaborate concentration during the hydrolysis of AB should also be taken into account.[50]

To better understand the hydrolysis of MeAB in the presence of $Ag_{0.1}@Co_{0.9}$/graphene NPs, and confirm the completely decomposed of MeAB after the catalytic reaction, we

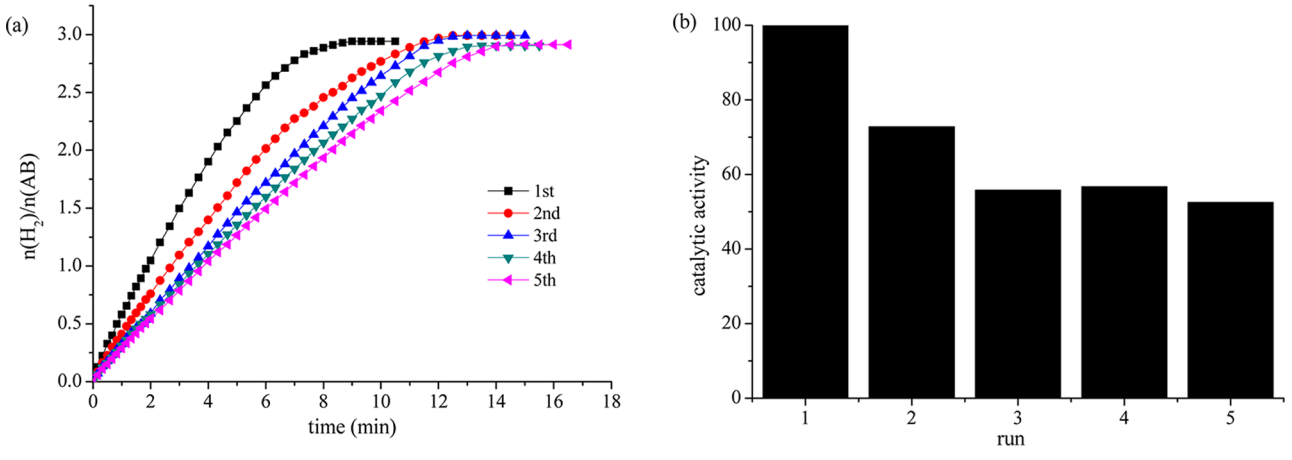

Figure 15. (a) Hydrogen generation from AB catalyzed by $Ag_{0.1}@Co_{0.9}$/graphene NPs from first to fifth cycles, catalyst/AB = 0.05; (b) percentage of initial catalytic activity of $Ag_{0.1}@Co_{0.9}$/graphene NPs in successive runs after the reuse for the hydrolysis of AB.

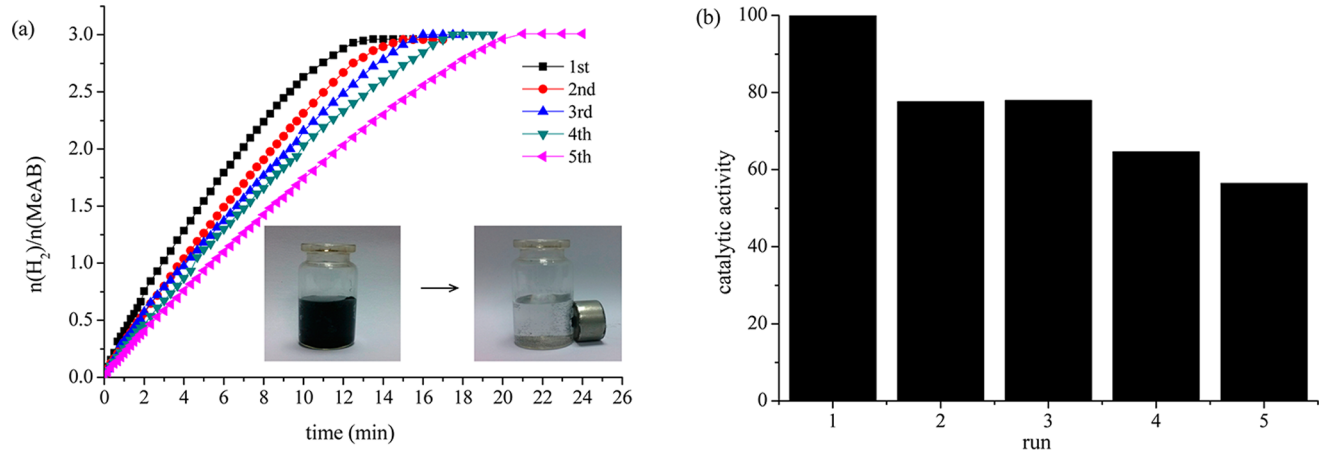

Figure 16. (a). Hydrogen generation from MeAB catalyzed by $Ag_{0.1}@Co_{0.9}$/graphene from first to fifth cycles, catalyst/MeAB = 0.05, and (inset) photographs of the $Ag_{0.1}@Co_{0.9}$/graphene NPs before (left) and after (right) the magnetic separation. (b) Percentage of initial catalytic activity of $Ag_{0.1}@Co_{0.9}$/graphene NPs in successive runs after the reuse for the hydrolysis of MeAB.

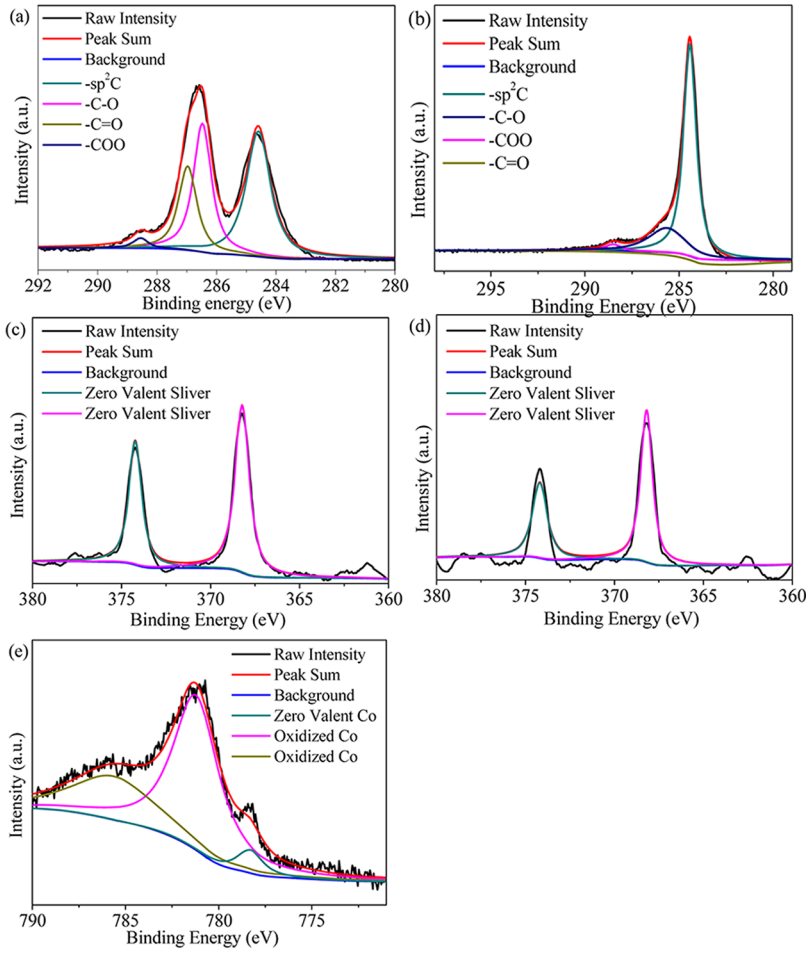

Figure 17. XPS spectra of (a, b) C1s of GO and graphene, (c, d) Ag 3d levels of $Ag_{0.1}@Co_{0.9}$/graphene NPs before and after five cycles, (e) Co 2p after five cycles.

performed the ^{11}B NMR studies (Figure 18). The ^{11}B peak at −19.8 ppm which assigned to MeAB is disappeared after the catalytic reaction, and a new peak around 11.4 ppm is observed indicating three moles of hydrogen has been generated from the one mole of MeAB via the catalytic hydrolysis according to eq 1. Furthermore, there is no change in the ^{11}B NMR of the MeAB after stay 7 days under ambient condition, indicating the catalytic activity of the as-prepared NPs toward catalytic hydrolysis of MeAB at ambient condition.

4. CONCLUSION

In summary, we have development a facile in situ one-step method for the synthesis of magnetic graphene supported Ag@M (M = Co, Ni, Fe) core−shell NPs with MeAB as the

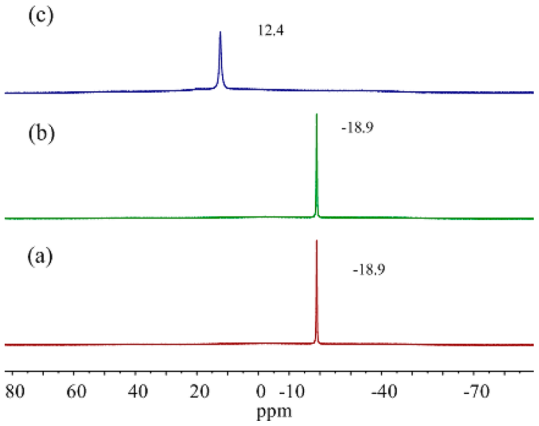

Figure 18. ^{11}B NMR spectra of (a) aqueous MeAB solution freshly prepared, (b) aqueous MeAB solution after 7 days under air, (c) aqueous MeAB solution after catalyzed by $Ag_{0.1}@Co_{0.9}$/graphene NPs.

reducing agent, and their catalytic activities toward hydrolytic dehydrogenation of AB under ambient condition were studied. The Ag@Co/graphene NPs exhibit superior catalytic activity, with the turnover frequency (TOF) value of 102 (mol H_2 min^{-1} (mol Ag)$^{-1}$), and activation energy (E_a) of 20.03 kJ/mol; follow by Ag@Ni/graphene NPs, whereas the Ag@Fe/graphene NPs are almost inactive. Compared with AB and $NaBH_4$, the as-synthesized Ag@Co/graphene catalysts reduced by MeAB exert the highest catalytic activity. The graphene supported Ag@Co NPs exhibit higher catalytic activity than the SiO_2, carbon black, and γ-Al_2O_3 supported or graphene-free counterparts. Furthermore, the as-synthesized Ag@Co/graphene NPs show good durable stability and magnetically recyclability for the hydrolytic dehydrogenation of AB and MeAB, which makes the practical recycling application of the catalyst more convenient. Moreover, this simple synthetic method can be extended to other graphene-supported core−shell NPs systems in more applications.

AUTHOR INFORMATION

Corresponding Author

*E-mail: wluo@whu.edu.cn (W.L.); gzcheng@whu.edu.cn (G.C.). Tel.: +86 2787467716.

Notes

The authors declare no competing financial interest.

ACKNOWLEDGMENTS

This work was financially supported by the National Natural Science Foundation of China (21201134), the Ph. D Programs Foundation of Ministry of Education of China (20120141120034), and Large-scale Instrument and Equipment Sharing Foundation of Wuhan University.

REFERENCES

(1) Kesavan, K.; Tiruvalam, R.; Rahim, M. H. A.; Saiman, M. I.; Enache, D. I.; Jenkins, R. L.; Dimitratos, N.; Lopez-Sanchez, J. A.; Taylor, S. H.; Knight, D. W.; Kiely, C. J.; Hutchings, G. J. *Science* **2011**, *331*, 195−199.
(2) Chaudhuri, R. G.; Paria, S. *Chem. Rev.* **2012**, *112*, 2373−2433.
(3) Ferrando, R.; Jellinek, J.; Johnston, R. L. *Chem. Rev.* **2008**, *108*, 845−910.
(4) Sekol, R. C.; Li, X. K.; Cohen, P.; Doubek, G.; Carmo1, M.; Taylor, A. D. *Appl. Catal., B* **2013**, *138−139*, 285−293.
(5) Xu, D.; Liu, Z. P.; Yang, H. Z.; Liu, Q. S.; Zhang, J.; Fang, J. Y.; Zou, S. Z.; Sun, K. *Angew. Chem., Int. Ed.* **2009**, *48*, 4217−4221.
(6) Lee, C.; Wei, X. D.; Kysar, J. W.; Hone, J. *Science* **2008**, *321*, 385−388.
(7) Novoselov, K. S.; Geim, A. K.; Morozov, S. V.; Zhang, Y.; Dubonos, S. V.; Grigorieva, I. V.; Firsov, A. A. *Science* **2004**, *306*, 666−669.
(8) Garaj, S.; Hubbard, W.; Reina, A.; Kong, J.; Branton, D.; Golovchenko, J. A. *Nature* **2010**, *467*, 190−194.
(9) Choi, B. G.; Hong, J.; Park, Y. C.; Jung, D. H.; Hong, W. H.; Hammond, P. T.; Park, H. S. *ACS Nano* **2011**, *5*, 5167−5174.
(10) Guo, S. J.; Sun, S. H. *J. Am. Chem. Soc.* **2012**, *134*, 2492−2495.
(11) Mazumder, V.; Chi, M. F.; More, K. L.; Sun, S. H. *Angew. Chem., Int. Ed.* **2010**, *49*, 9368−9372.
(12) Vinodgopal, K.; Neppolian, B.; Lightcap, I. V.; Grieser, F.; Ashokkumar, M.; Kamat, P. V. *J. Am. Chem. Soc.* **2010**, *1*, 1987−1993.
(13) Liu, C. B.; Wang, K.; Luo, S. L.; Tang, Y. H.; Chen, L. Y. *Small* **2011**, *7*, 1203−1206.
(14) Tang, X. Z.; Cao, Z. W.; Zhang, H. B.; Liu, J.; Yu, Z. Z. *Chem. Commun.* **2011**, *47*, 3084−3086.
(15) Zhang, K.; Yue, Q. L.; Chen, G. F.; Zhai, Y. L.; Wang, L.; Wang, H. S.; Zhao, J. S.; Liu, J. F.; Jia, J. B.; Li, H. B. *J. Phys. Chem.* **2011**, *115*, 379−389.
(16) Graetz, J. *Chem. Soc. Rev.* **2009**, *38*, 73−82.
(17) Suh, M. P.; Park, H. J.; Prasad, T. K.; Lim, D. W. *Chem. Rev.* **2012**, *112*, 782−835.
(18) Staubitz, A.; Robertson, A. P. M.; Manners, I. *Chem. Rev.* **2010**, *110*, 4079−4124.
(19) Luo, W.; Campbell, P. G.; Zakharov, L. N.; Liu, S. Y. *J. Am. Chem. Soc.* **2011**, *133*, 19326−19329.
(20) Gutowska, A.; Li, L. Y.; Shin, Y.; Wang, C. M.; Li, X. H. S.; Linehan, J. C.; Smith, R. S.; Kay, B. D.; Schmid, B.; Shaw, W.; Gutowski, M.; Autrey, T. *Angew. Chem., Int. Ed.* **2005**, *44*, 3578−3582.
(21) Xiong, Z. T.; Yong, C. K.; Wu, G. T.; Chen, P.; Shaw, W.; Karkamkar, A.; Autery, T.; Jones, M. O.; Johnson, S. R.; Edwards, P. P.; David, W. I. F. *Nat. Mater.* **2008**, *7*, 138−141.
(22) Blaquiere, N.; Diallo-Garcia, S.; Gorelsky, S. I.; Black, D. A.; Fagnou, K. *J. Am. Chem. Soc.* **2008**, *130*, 14034−14035.
(23) Durap, F.; Zahmakıran, M.; Özkar, S. *Appl. Catal., A* **2009**, *369*, 53−59.
(24) Liang, H. Y.; Chen, G. Z.; Desinan, S.; Rosei, R.; Rosei, F.; Ma, D. L. *Int. J. Hydrogen Energy* **2012**, *37*, 17921−17927.
(25) Rakapa, M.; Kalua, E. E.; Özkar, S. *J. Power Sources* **2012**, *210*, 184−190.
(26) Yan, J. M.; Wang, Z. L.; Wang, H. L.; Jiang, Q. *J. Mater. Chem.* **2012**, *22*, 10990−10993.
(27) Akbayrak, S.; Özkar, S. *ACS Appl. Mater. Interfaces* **2012**, *4*, 6302−6310.
(28) Can, H.; Metin, Ö. *Appl. Catal., B* **2012**, *125*, 304−310.
(29) Dai, H. B.; Gao, L. L.; Liang, Y.; Kang, X. D.; Wang, P. *J. Power Sources* **2010**, *195*, 307−312.
(30) Yamamoto, Y.; Miyamoto, K.; Umeda, J.; Nakatani, Y.; Yamamoto, T.; Miyaura, N. *J. Organomet. Chem.* **2006**, *691*, 4909−4917.
(31) Staubitz, A.; Sloan, M. E.; Robertson, A. P. M.; Friedrich, A.; Schneider, S.; Gates, P. J.; Günne, J. S.; Manners, I. *J. Am. Chem. Soc.* **2010**, *132*, 13332−13345.
(32) Kalidindi, S. B.; Sanyal, U.; Jagirdar, B. R. *ChemSusChem* **2011**, *4*, 317−324.
(33) Sanyal, U.; Davis, D. T.; Jagirdar, B. R. *Dalton Trans.* **2013**, *42*, 7147−7157.
(34) Hummers, W.; Offeman, R. *J. Am. Chem. Soc.* **1958**, *80*, 1339−1399.
(35) Kovtyukhova, N. I.; Ollivier, P. J.; Martin, B. R.; Mallouk, T. E.; Buzaneva, E. V.; Gorchinskiy, A. D. *Chem. Mater.* **1999**, *11*, 771−778.
(36) Yang, Z. X.; Cheng, F. Y.; Tao, Z. L.; Liang, J.; Chen, J. *Int. J. Hydrogen Energy* **2012**, *37*, 7638−7644.
(37) Figen, A. K.; Coşkuner, B. *Int. J. Hydrogen Energy* **2013**, *38*, 2824−2835.

(38) Jiang, H. L.; Akita, T.; Xu, Q. *Chem. Commun.* **2011**, *47*, 10999−11001.
(39) Wang, J.; Qin, Y. L.; Liu, X.; Zhang, X. B. *J. Mater. Chem.* **2012**, *22*, 12468−12470.
(40) Yan, J. M.; Zhang, X. B.; Han, S.; Shioyama, H.; Xu, Q. *Angew. Chem., Int. Ed.* **2008**, *47*, 2287−2289.
(41) Chen, G. Z.; Desinan, S.; Rosei, R.; Rosei, F.; Ma, D. L. *Chem.—Eur. J.* **2012**, *18*, 7925−7930.
(42) Metin, Ö.; Sahin, S.; Özkar, S. *Int. J. Hydrogen Energy* **2009**, *34*, 6304−6313.
(43) Chen, G. Z.; Desinan, S.; Nechache, R.; Rosei, R.; Roseiacd, F.; Ma, D. L. *Chem. Commun.* **2011**, *47*, 6308−6310.
(44) Durap, F.; Zahmakıran, M.; Özkar, S. *Int. J. Hydrogen Energy* **2009**, *34*, 7223−7230.
(45) Rachiero, G. P.; Demirci, U. B.; Miele, P. *Int. J. Hydrogen Energy* **2011**, *36*, 7051−7065.
(46) Rachiero, G. P.; Demirci, U. B.; Miele, P. *Catal. Today* **2011**, *170*, 85−92.
(47) Sun, B. L.; Wen, M.; Wu, Q. S.; Peng, J. *Adv. Funct. Mater.* **2012**, *22*, 2860−2866.
(48) Xi, P. X.; Chen, F. J.; Xie, G. Q.; Ma, C.; Liu, H. Y.; Shao, C. W.; Wang, J.; Xu, Z. H.; Xu, X. M.; Zeng, Z. Z. *Nanoscale* **2012**, *4*, 5597−5601.
(49) Wen, M.; Sun, B. L.; Zhou, B.; Wu, Q. S.; Peng, J. *J. Mater. Chem.* **2012**, *22*, 11988−11993.
(50) Chandra, M.; Xu, Q. *J. Power Sources* **2006**, *156*, 190−194.